

High pressure structural and elastic properties of NiO up to 67 GPaL. Liu,^{1,3} X. D. Li,¹ J. Liu,^{1,a)} S. Jiang,¹ Y. C. Li,¹ G. Y. Shen,² H. K. Mao,² Y. Bi,³ and J. Xu³¹Beijing Synchrotron Radiation Facility, Institute of High Energy Physics, Chinese Academy of Sciences, Beijing 100049, China²HPCAT, Advanced Photon Source, Argonne National Laboratory, Argonne, Illinois 60439, USA and Geophysical Laboratory, Carnegie Institution of Washington, Washington DC 20015, USA³Laboratory for Shock Wave and Detonation Physics Research, Institute of Fluid Physics, Mianyang 621900, China

(Received 6 August 2008; accepted 9 October 2008; published online 9 December 2008)

Using argon as the pressure medium, the structural and elastic properties of NiO have been investigated up to 67 GPa by the *in situ* synchrotron x-ray diffraction in a diamond anvil cell. Up to 67 GPa, NiO remains in the rhombohedral distorted rocksalt structure without phase transition. The lattice parameters of a and c , indexed in the hexagonal lattice, were found to decrease monotonically with increasing pressure, while the c/a ratio remains almost constant. The elastic properties of NiO were studied by analyzing the linewidth of various diffraction peaks, which indicates that the factor $S=(S_{11}-S_{12}-S_{44}/2)$ is negative although the single-crystal elastic compliances S_{11} is positive, respectively, in the investigated pressure range.

© 2008 American Institute of Physics. [DOI: 10.1063/1.3031697]

I. INTRODUCTION

The 3d transition-metal monoxides such as NiO are of considerable interest because of manifold electronic and magnetic phenomena.¹⁻³ As a prototype of Mott insulator, the electronic and magnetic properties of NiO at ambient pressure were investigated by many groups⁴⁻¹⁰ in the past decades. However, the structure evolution and elastic properties of NiO under high pressure have not been well understood.

NiO is a well known antiferromagnetic material with the Néel temperature (T_N) of 523 K. NiO has a cubic rocksalt structure ($B1$) above T_N . Below T_N , NiO transforms to a rhombohedral distorted rocksalt structure ($rB1$) by a compression along the body diagonal direction with the rhombohedral angle α_{rh} of 60.08°, which is close to 60.00° in the undistorted lattice. No phase transition has been found under high pressure up to 147 GPa in experimental investigations.¹¹⁻¹³ In 1996, Sasaki¹⁴ investigated the structure evolution of NiO under high pressure within the density functional formalism with the local spin density approximation (LSDA). He found that the lattice parameters of a and c , indexed in the hexagonal system, and the c/a ratio decrease monotonically with pressures, but the pressure derivatives of c/a become significantly large above 60 GPa. He also predicted that NiO transforms to CsCl structure ($B2$) at 318 GPa. Eto *et al.*¹³ compressed NiO powder in a diamond anvil cell (DAC) up to 141 GPa and found that the pressure coefficient of c/a almost remains constant in the investigated pressure range. Recently, Zhang *et al.*^{15,16} investigated the structure properties of NiO with generalized gradient approximation (GGA) by taking the strong electronic correlations into account. They gave the accordant results with Eto

et al. and the phase transition from the distorted rocksalt to the $B2$ structure was calculated to occur at 410 GPa. In the experiments of Eto *et al.*, the solution of methanol-ethanol was used as a pressure medium, which has a large deviatoric stress in the sample chamber at pressures over 10 GPa. Such deviatoric stress might influence the structure evolution of crystal structure under pressure.^{17,18} By using a better pressure medium, one of the goals of this work is to revisit the structure of NiO at high pressures. Furthermore, we report first results on the elastic behavior of NiO under high pressures.

II. EXPERIMENT

A modified Mao–Bell DAC was used to generate high pressure. Flat anvil with a culet size of 300 μm was used in all runs of experiments. The initial thickness of a preindented stainless steel T301 gasket and the diameter of the central hole were 30 and 100 μm , respectively. The powder sample of NiO (Alfa Aesar, purity of 99.998%) was loaded into the chamber with argon as the pressure medium. The x-ray diffraction experiments were performed at the HP-Station, 4W2 beamline at Beijing Synchrotron Radiation Facility (BSRF) and HPCAT, beamline 16-ID-B at the Advanced Photon Source (APS). For the experiments at BSRF, the energy dispersive method was used for diffraction measurements (run A). Spectra were collected using a solid-state Ge detector (IGLET-11145, ORTEC) with a multichannel analyzer at the diffraction angle 2θ of 21.96°, with acquiring time about 10 min. The x-ray beam was focused to a beam size of 20(vertical) \times 30(horizontal) μm^2 full width at half maximum by Kirkpatrick–Baez mirrors. Ruby chips were loaded into the sample chamber for pressure measurement.¹⁹ For the experiment at APS, the monochromatic synchrotron x radiation ($\lambda=0.3931$ Å) at 16-ID-B beamline was used for the angle-dispersive x-ray diffraction (ADX) measurement

^{a)}Author to whom correspondence should be addressed. Electronic mail: liuj@ihep.ac.cn.

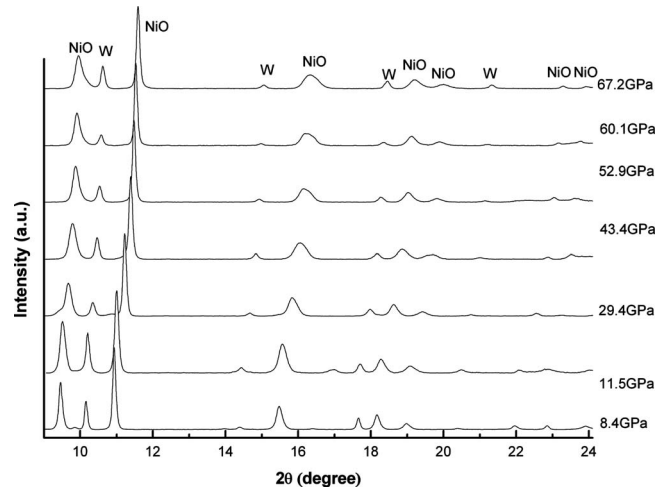


FIG. 1. The representative patterns of ADXD experiments of NiO.

(run B). An image plate detector (MAR3450) was used to collect diffraction patterns. CeO_2 standard was used to calibrate the sample to detector distance and the detector tilt. Tungsten powder was mixed with NiO acting as pressure standard.²⁰ All of the measurements were conducted at ambient temperature and the pressures were gradually increased up to 66 GPa for run A and up to 67 GPa for run B.

III. RESULTS AND DISCUSSIONS

A. Structure behavior

Figure 1 shows the representative patterns of ADXD measurements of NiO. No structural phase transition is observed in the pressure range, in contrast to other transition metal monoxides [such as FeO (Ref. 21) MnO (Ref. 22)], which shows structural transformations at high pressure to NiAs structure (*B8*). The diffraction peaks remain sharp with only slightly broadening with pressure, suggesting that non-hydrostatic stress was small at high pressure in argon pressure medium.

The evolution of lattice parameters c and a , expressed in the hexagonal lattice, and the c/a ratio with pressure are illustrated in Fig. 2, together with experimental data from Eto *et al.*,¹³ LSDA results calculated by Sasaki,¹⁴ and GGA+ U results performed by Zhang *et al.*¹⁵ for comparison. In our experiment, the lattice parameters a and c are optimized by taking all diffracted peaks into account, the relative uncertainty of the lattice parameters are smaller than 4×10^{-3} . The values of c and a decrease monotonically and the c/a ratio remains the same within experimental uncertainties in the entire pressure range investigated in our experiment, which is different from the LSDA result with a mutation above 60 GPa. The GGA+ U results are consistent with the trend of our results, although the pressure coefficients of c , a , and c/a in GGA+ U are slightly larger. The values of a agree well with Eto's experimental results, but the values of c in this study decrease at a slower rate than those from Eto *et al.* The c/a ratio of this study remains 2.449(5), which is close to the theoretical value of c/a ratio of *B1* structure in the pressure range. In the data process, the resulted $d(c/a)/dP$ is less than its standard deviation of 1.4×10^{-5} . The major dif-

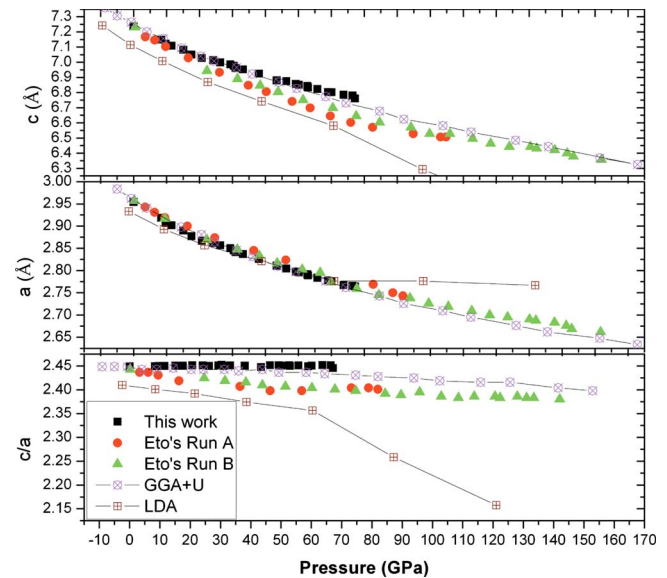


FIG. 2. (Color online) Pressure dependence of structure parameters c , a , and the axial ratio c/a together with the published results from experiment, GGA+ U calculation, and LSDA calculation.

ference between the Eto *et al.* and our experiments is that we used argon as pressure media while they used the solution of methanol-ethanol. Argon usually serves as a better hydrostatic medium than methanol-ethanol.^{23–26} Additionally, Eto *et al.* used rhenium gasket for pressure measurement, which could underestimate the pressure by about several GPa.

B. Equation of state (EOS)

Figure 3 illustrates the pressure dependence of volume of a hexagonal unit cell together with the experiment results by Eto *et al.*,¹³ Huang *et al.*,¹¹ and Noguchi *et al.*,¹² respectively. The present results are consistent with previous experiment results and calculation results using GGA+ U at pressures below 40 GPa. However above that pressure, the discrepancy appears: the present results reveal less compressible at high pressure. We fit the present ADXD data

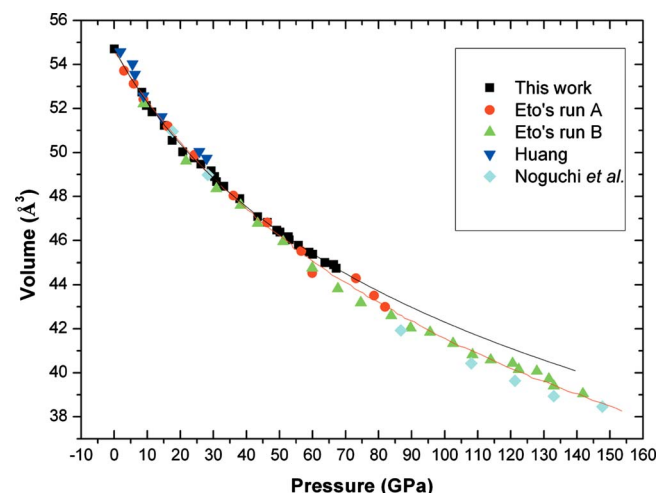


FIG. 3. (Color online) Pressure dependence of a hexagonal unit cell of NiO, together with the experiment results from Refs. 11–13. The black line is the fitting of our ADXD result to the third-order Birch–Murnaghan EOS. The red line is the fitting of Eto's results.

TABLE I. Bulk modulus B_0 and pressure derivative of the bulk modulus B'_0 .

	V_0	B_0 (GPa)	B'_0	Pressure range (GPa)	Pressure media
GGA+U ^a	55.22	184	4.93	0–9.04	...
		189	3.91	0–64.2	...
		193	3.67	0–147.3	...
LSDA ^b	52.83	236	4.28	0–60	...
		192(4)	4.0	0–9.3	4:1Methanol-ethanol
Eto <i>et al.</i> ^c	54.66	203(2)	4.0	0–60.1	4:1Methanol-ethanol
		210(2)	4.0	0–141.7	4:1Methanol-ethanol
		187	4.0	0–6.6	4:1Methanol-ethanol
Huang ^d		187	4.0	0–6.6	4:1Methanol-ethanol
Noguchi <i>et al.</i> ^e		191	3.9	0–147.6	...
This work(run A)		188(4)	4.0	0–65.9	Argon
This work(run B)	54.70(2)	195(4)	5.3(2)	0–67.2	Argon
This work(run B)	54.70(2)	189(4)	4.0	0–11.5	Argon

^aReference 15.^bReference 14.^cReference 13.^dReference 11.^eReference 12.

points with the third-order Brich–Murnaghan EOS resulting in a bulk modulus of $B_0=195(4)$ GPa with its pressure derivative $B'_0=5.3(2)$ (Table I). The ambient volume V_0 was then fixed at our determined value of 54.70 \AA^3 during the whole data set fitting. This volume is close to Eto's result (54.66 \AA^3) while bigger than the LSDA result of 52.83 \AA^3 (Ref. 14) and smaller than the GGA+ U result of 55.22 \AA^3 .¹⁵ The observed B_0 below 10 GPa gives a consistent result with both of Eto and Huang's results when the methanol-ethanol mixture serves as a hydrostatic medium. Huang pointed out that the value of the bulk modulus obtained under a nonhydrostatic environment tended to be higher than those obtained under a hydrostatic environment because of shear stress. We obtained the bulk modulus consistent with Eto though the hydrostaticity in our experiment was better. This could be explained by the pressure determination as mentioned in Sec. III A.

C. Constraints on elasticity

For simplicity, all the peaks are indexed into a cubic system in this section in order to investigate the elastic properties of NiO. Plessis *et al.*²⁷ considered that the small rhombohedral distortion leads only to a negligible contribution to the elastic constants so it is practical ignoring the distortion and taking it as cubic when discussing the elastic properties.

The lattice parameter for a cubic system determined from different reflections recorded with the conventional geometry satisfies the following equation:²⁸

$$a_m = M_0 + M_1[3\Gamma(hkl)(1 - 3 \cos^2 \Psi)], \quad (1)$$

where

$$M_0 = a_p \{1 + (\alpha t/3)(1 - 3 \sin^2 \theta)[(S_{11} - S_{12}) - (1 - \alpha^{-1}) \times (2G_V)^{-1}]\},$$

$$M_1 = -a_p(\alpha St/3),$$

$$\Gamma(hkl) = (h^2k^2 + k^2l^2 + l^2h^2)/(h^2 + k^2 + l^2)^2,$$

$$S = (S_{11} - S_{12} - S_{44}/2),$$

a_m and a_p are the determined lattice constant, and the lattice constant under hydrostatic pressure accordingly. The S_{ij} are the single-crystal elastic compliances under pressure and θ is the diffraction angle. α determines the relative weights of the isostress and isostrain condition across the grain boundary in an actual case and G_V is the shear modulus under isostrain condition. t denotes the differences between the axial and radial stresses termed as uniaxial stress component.

In conventional diffraction geometry as shown in Fig. 4, $\Psi = \pi/2 - \theta$, Eq. (1) can be rewritten

$$a_m = M_0 + M_1[3\Gamma(hkl)(1 - 3 \sin^2 \theta)]. \quad (2)$$

As discussed in Ref. 29, $M_0 \approx a_p$ and the a_m versus $3\Gamma(hkl)(1 - 3 \sin^2 \theta)$ plot termed as gamma plot is a straight line. This suggests an effective method to estimate the value of t

$$\alpha t S = -3M_1/M_0. \quad (3)$$

On the basis of the breadth due to grain size varies with angle as $1/\cos \theta$ and that due to strain as $\tan \theta$, Langford³⁰ gave the following relation:

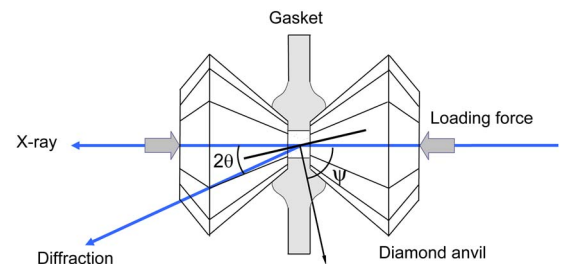


FIG. 4. (Color online) Conventional diffraction geometry.

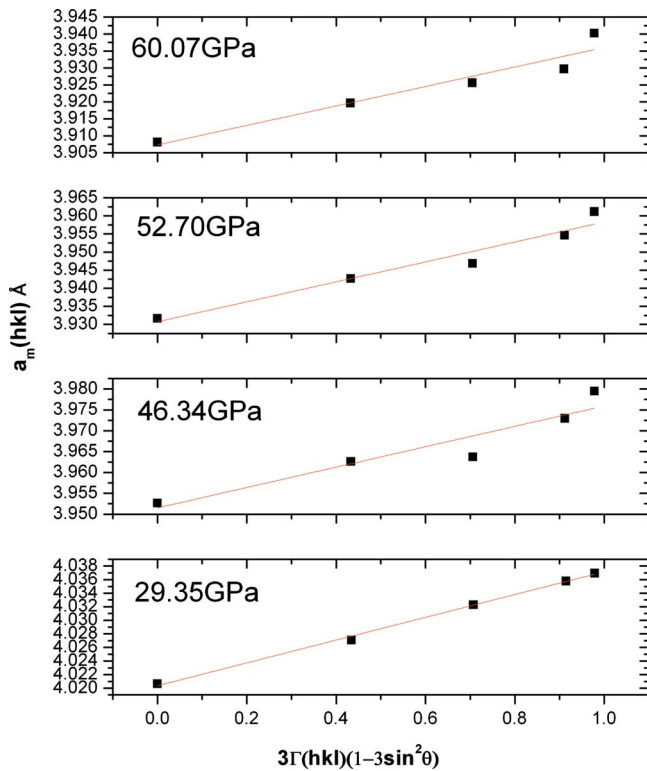


FIG. 5. (Color online) Examples of gamma plot.

$$(2w_{hkl} \cos \theta_{hkl})^2 = (\lambda/d)^2 + \eta_{hkl}^2 \sin^2 \theta_{hkl}. \quad (4)$$

Here $2w_{hkl}$, θ_{hkl} , λ , d , and η_{hkl} denote the linewidth, Bragg angle, x-ray wavelength, grain size (assumed to be hkl independent), and microstrain, respectively.

The hkl dependent of η_{hkl} can be obtained by the following relation:

$$\eta_{hkl} = 4P_{\max}[S_{11} - 2S\Gamma(hkl)], \quad (5)$$

and high pressure studies on magnesium oxide,³¹ gold,³² and iron³³ show that $2P_{\max} = t$ so,

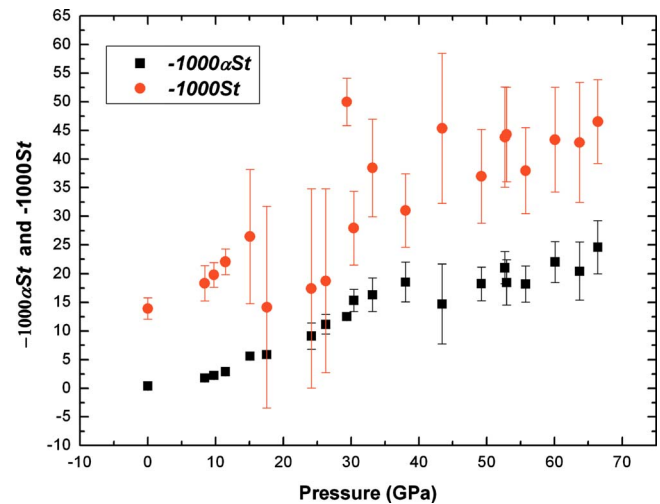
$$\eta_{hkl} = 2t[S_{11} - 2S\Gamma(hkl)]. \quad (6)$$

The examples of gamma plot are illustrated in Fig. 5. All the slope and intercept are positive so the values of αSt are negative from Eq. (3). Note that α and t are positive by convention, this result shows that S for NiO is negative in the pressure range investigated. The elastic anisotropy of a cubic crystal can be characterized by the Zener anisotropy ratio A ,

$$A = \frac{C_{44}}{1/2(C_{11} - C_{12})} = \frac{(S_{11} - S_{12})}{1/2S_{44}}. \quad (7)$$

If $S < 0$, $A > 1$, it indicates that the shear moduli of NiO in the (100) plane along [100] direction is larger than in the (110) plane along [100] direction.

The αSt values calculated using Eq. (3) is shown in Fig. 6: the absolute values of αSt increase with pressure but the slope becomes smaller above 30 GPa while the errors get larger. By fitting $\sin^2 \theta_{hkl}$ versus $(2w_{hkl} \cos \theta_{hkl})^2$ data, grain size d and microstrain η_{hkl} are obtained. Figure 7 shows the grain size under different pressures and suggests its independence with pressure in this experiment. The $S_{11}t$ and St cal-

FIG. 6. (Color online) αSt values derived from the gamma plots and St values derived from the analysis of linewidth at different pressure.

culated from Eq. (6) are illustrated in Figs. 6 and 8,, respectively. They indicate positive S_{11} and negative S consistent with the value calculated using Eq. (3). Both of them exhibit rising trend with pressure.

Since the linewidth $2w_{hkl}$ has not been corrected for instrumental effects, the grain sizes are underestimated systematically. Instrumental effects would lead to the broadening of the diffraction lines $w \sim 10^{-30}$, while $\lambda/d \sim 10^{-3}$, so the error of d is comparable to the value d . However this would not affect the trend of the value of d with pressure. Contrast to η_{hkl} , instrumental effects are very small and can be ignored.

IV. CONCLUSIONS

The powder of NiO was hydrostatically compressed up to 67 GPa. No structural phase transition was observed in the pressure range. The pressure coefficient of axial ratio c/a , $-d(c/a)/dP$ in hydrostatic environment is smaller than the non-hydrostatic compression data and the prediction based on calculation by LSDA. Accordingly, the bulk modulus B_0 is in good agreement with previous experiments by Eto *et al.* We

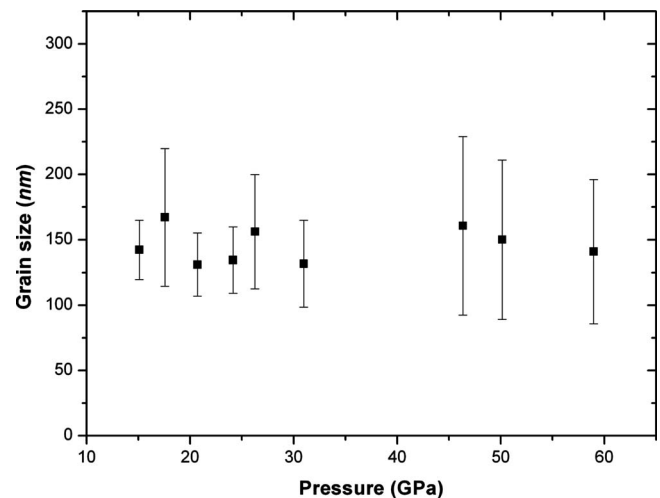


FIG. 7. The grain sizes under different pressure, showing independence with pressure.

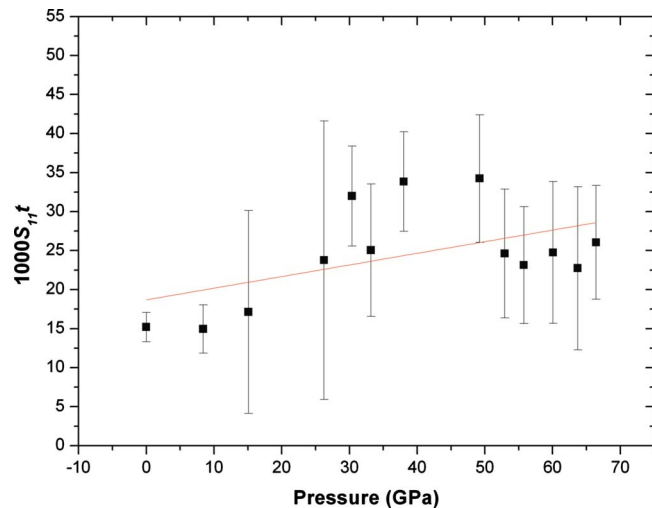


FIG. 8. (Color online) $S_{11}t$ values derived from the analysis of linewidth at different pressure. The red line is plotted to guide the eyes.

analyze the linewidth under pressure and obtained the positive S_{11} and negative S , which indicates that the shear moduli of NiO in the (100) plane along the [100] direction is larger than that in the (110) plane along the [100] direction.

ACKNOWLEDGMENTS

The authors thank H. Z. Liu for assistance in the diffraction experiment, H. P. Liermann for the help in sample preparation, S.V. Sinogeikin for assistance in use of ruby system. This work was performed at HPCAT, APS, Argonne National Laboratory. Preliminary experiments were conducted at 4W2 High-Pressure Station of BSRF, which is supported by Chinese Academy of Sciences (Grant Nos. KJCX2-SW-N03 and KJCX2-SW-N20). Financial support from the National Natural Science Foundation of China (Grant No. 10676034), the Ministry of Science and Technology of China (Grant No. 2005CB724400) is gratefully acknowledged.

- ¹R. E. Cohen, I. I. Mazin and D. G. Issak, *Science* **275**, 654 (1997).
- ²Z. Fang, K. Terakura, H. Sawada, T. Miyazaki, and I. Solovyev *Phys. Rev. Lett.* **81**, 1027 (1998).
- ³C. S. Yoo, B. Maddox, J.-H. P. Klepeis, V. Iota, W. Evans, A. McMahan, M. Y. Hu, P. Chow, M. Somayazulu, D. Häusermann, R. T. Scalettar, and W. E. Pickett, *Phys. Rev. Lett.* **94**, 115502 (2005).
- ⁴A. K. Cheetham and D. A. O. Hope, *Phys. Rev. B* **27**, 6964 (1983).
- ⁵A. Svane and O. Gunnarsson, *Phys. Rev. Lett.* **65**, 1148 (1990).
- ⁶V. I. Anisimov, J. Zaanen, and O. K. Andersen, *Phys. Rev. B* **44**, 943 (1991).
- ⁷A. F. Aryasetiawan and O. Gunnarsson, *Phys. Rev. Lett.* **74**, 3221 (1995).
- ⁸S. L. Dudarev, G. A. Botton, S. Y. Savrasov, C. J. Humphreys, and A. P. Sutton, *Phys. Rev. B* **57**, 1505 (1998).
- ⁹A. Rohrbach, J. Hanner, and G. Kresse, *Phys. Rev. B* **69**, 075413 (2004).
- ¹⁰T. M. Schuler, D. L. Ederer, S. Itza-Ortiz, G. T. Woods, T. A. Callcott, and J. C. Woicik, *Phys. Rev. B* **71**, 115113 (2005).
- ¹¹E. Huang, *High Press. Res.* **13**, 307 (1995).
- ¹²Y. Noguchi, M. Uchino, H. Hikosaka, T. Atou, K. Kusaba, F. Fukuoka, T. Mashimo, and Y. Syono, *J. Phys. Chem. Solids* **60**, 509 (1999).
- ¹³T. Eto, S. Endo, M. Imai, Y. Katayama, and T. Kikegawa, *Phys. Rev. B* **61**, 14984 (2000).
- ¹⁴T. Sasaki, *Phys. Rev. B* **54**, R9581 (1996).
- ¹⁵W.-B. Zhang, Y.-L. Hu, K.-L. Han, and B.-Y. Tang, *Phys. Rev. B* **74**, 054421 (2006).
- ¹⁶W.-B. Zhang, Y.-L. Hu, K.-L. Han, and B.-Y. Tang, *J. Phys.: Condens. Matter* **18**, 9691 (2006).
- ¹⁷L. S. Dubrovinsky and A. B. Belonoshko, *Geochim. Cosmochim. Acta* **60**, 3657 (1996).
- ¹⁸W. Cao and J.A. Krumhansl, *Phys. Rev. B* **42**, 4334 (1990).
- ¹⁹H.-K. Mao, J. Xu, and P. Bell, *J. Geophys. Res.* **91**, 4673 (1986).
- ²⁰S. P. Marsh, Los Alamos Shock Hugoniot Data, 1979.
- ²¹Y. Fei and H. K. Mao, *Science* **266**, 1678 (1994).
- ²²T. Kondo, T. Yagi, and Y. Syono, *Rev. High Pressure Sci. Technol.* **7**, 148 (1998).
- ²³L. W. Finger, R. M. Hazen, G. Zou, H. K. Mao, and P. M. Bell, *Appl. Phys. Lett.* **39**, 892 (1981).
- ²⁴H. K. Mao, J. Badro, J. Shu, R.J. Hemley, A. K. Singh, *J. Phys.: Condens. Matter* **18**, S963 (2006).
- ²⁵G. J. Piermarini, S. Block, and J. D. Barnett, *J. Appl. Phys.* **44**, 5377 (1973).
- ²⁶T. Kenichi and A. K. Singh, *Phys. Rev. B* **73**, 224119 (2006).
- ²⁷P. V. Plessis, S. J. Tander, and L. Alberts, *J. Phys. C* **4**, 1983 (1971).
- ²⁸A. K. Singh and C. Balasingh, *J. Appl. Phys.* **83**, 7567 (1998).
- ²⁹A. K. Singh, *J. Appl. Phys.* **90**, 3269 (2001).
- ³⁰J. I. Langford, *J. Appl. Crystallogr.* **4**, 164 (1971).
- ³¹A. K. Singh, H. P. Liermann, and S. K. Saxena, *Solid State Commun.* **132**, 795 (2004).
- ³²A. K. Singh, H. P. Liermann, S. K. Saxena, H. K. Mao, and S. Usha Devi, *J. Phys.: Condens. Matter* **18**, S969 (2006).
- ³³A. K. Singh, A. Jain, H. P. Liermann, and S. K. Saxena, *J. Phys. Chem. Solids* **67**, 2197 (2006).